A Journal of the Gesellschaft Deutscher Chemiker

Angewandte International Edition

GDCh

Chemie

www.angewandte.org

Accepted Article

Title: Defect-Rich Bi12O17Cl2 Nanotubes Self-Accelerating Charge Separation for Boosting Photocatalytic CO2 Reduction

Authors: Jun Di, Chao Zhu, Mengxia Ji, Meilin Duan, Ran Long, Cheng Yan, Kaizhi Gu, Jun Xiong, Yuanbin She, Jiexiang Xia, Huaming Li, and Zheng Liu

To be cited as: *Angew. Chem. Int. Ed.* 10.1002/anie.201809492
Angew. Chem. 10.1002/ange.201809492

Link to VoR: http://dx.doi.org/10.1002/anie.201809492
http://dx.doi.org/10.1002/ange.201809492

WILEY-VCH

10.1002/anie.201809492

Defect-Rich $Bi_{12}O_{17}Cl_2$ Nanotubes Self-Accelerating Charge Separation for Boosting Photocatalytic CO_2 Reduction

Jun Di[1,2‡], Chao Zhu[2‡], Mengxia Ji[1], Meilin Duan[3], Ran Long[3], Cheng Yan[2], Kaizhi Gu[4], Jun Xiong[1], Yuanbin She[5], Jiexiang Xia[1,*], Huaming Li[1], Zheng Liu[2,*]

[1] School of Chemistry and Chemical Engineering, Institute for Energy Research, Jiangsu University, 301 Xuefu Road, Zhenjiang, 212013, P. R. China

[2] Center for Programmable Materials, School of Materials Science & Engineering, Nanyang Technological University, Singapore 639798, Singapore

[3] Hefei National Laboratory for Physical Sciences at the Microscale, School of Chemistry and Materials Science, and National Synchrotron Radiation Laboratory, University of Science and Technology of China, Hefei, Anhui 230026, P. R. China

[4] School of Chemistry and Molecular Engineering, East China University of Science and Technology, Shanghai 200237, P. R. China

[5] College of Chemical Engineering, Zhejiang University of Technology, Hangzhou, 310032, P. R. China

‡ These authors contributed equally to this work.

*Corresponding author: z.liu@ntu.edu.sg; xjx@ujs.edu.cn

10.1002/anie.201809492

Abstract

Solar-driven reduction of CO_2, that converts inexhaustible solar energy to value-added fuels, has been recognized as a promising sustainable energy conversion technology. However, the overall conversion efficiency is significantly limited by the inefficient charge separation and sluggish interfacial reaction dynamic resulted from lacking sufficient active sites. Herein, $Bi_{12}O_{17}Cl_2$ superfine nanotubes with bilayer thickness of tube wall are designed to achieve structural distortion for the creation of surface oxygen defects, thus accelerate carrier migration and facilitate CO_2 activation simultaneously. Without cocatalyst and sacrifice reagent, $Bi_{12}O_{17}Cl_2$ nanotubes deliver a high selectivity CO evolution rate of 48.6 μmol g^{-1} h^{-1} in water, roughly 16.8 times than that of bulk $Bi_{12}O_{17}Cl_2$. Meanwhile the nanotubes maintain their photocatalytic activity even after 12 h testing. This excellent activity is ascribed to better adsorption and activation of CO_2, increased separation efficiency of electron-hole pairs for both bulk and surface, as well as better CO liberation from catalyst. This work paves the way to design efficient photocatalysts with collaborative optimizing charge separation and CO_2 activation towards CO_2 photoreduction.

Keywords: $Bi_{12}O_{17}Cl_2$ nanotube; Oxygen defects; CO_2 reduction; Photocatalytic; Charge separation

10.1002/anie.201809492

With the drastic consumption of traditional fossil fuels, the energy crisis and environmental pollution have become serious problems worldwide.[1] Photocatalytic reduction of CO_2 has been considered as a promising alternative solution in the manner by converting inexhaustible solar energy to value-added fuels. During the past decades, numerous efforts have been devoted to the development of efficient photocatalysts with different structures for efficient CO_2 photoreduction.[2, 3] Despite certain progresses have been acquired, the CO_2 conversion efficiency is still fairly low, principally due to the high CO_2 activation energy, and the sluggish kinetics of involved multiple electrons and protons transfer processes. In order to achieve an efficient CO_2 conversion rate, boosting the charge separation efficiency and building active sites for facilitating CO_2 activation may be feasible approaches.

With the intense studies of layered materials, some functional 2D structures have attracted massive interest not only in electronic devices but also in catalysis application.[4-7] The high surface area enables better harvesting of solar energy, and the atom-thick layers allow the photogenerated charge carriers to migrate faster from the interior to the surface with less bulk recombination.[8] Benefit from these advantages, a series of ultrathin materials, such as g-C_3N_4,[9] In_2O_3,[10] Bi_2WO_6,[11] ZnAl-LDHs[12] and $ZnIn_2S_4$,[13] have been produced and widely investigated in the photocatalysis field. However, in spite of numerous researches on the optimization of ultrathin layered structures, the photocatalytic behavior is still unsatisfactory due to the high surface charge recombination rate and the lack of sufficient surface active sites. For instance in CO_2 reduction process, electrons generated in the interior of semiconductor first migrate to the surface and then activate the adsorbed CO_2 at active sites. Although the ultrathin structure reduces the recombination in the bulk, the surface-reached electrons will still recombine with holes, lying in the fact that insufficient active sites at surface can cause the sluggish interfacial reaction. To address aforementioned issues, building surface active sites for CO_2 activation and accelerating surface charge separation are necessary. Previous reports have demonstrated that the oxygen defects on the surface of photocatalysts are helpful for promoting the adsorption and activation of target molecules (e.g. N_2, O_2, CO_2).[14-16] By virtue of the increased local charge density at the

defect sites, these target molecules can create powerful interaction at oxygen defects, lower the bond energy of molecules and facilitate the transfer of photoexcited electrons to reaction species.[14, 17] Therefore, building surface oxygen defects is an important way to realize more active sites for high-efficiency CO_2 photoreduction.

Considering the intrinsic layered structure feature of 2D materials, if the 2D materials can be curved to form tubular structure, it will inevitably result in surface structure distortion. This structural distortion will lead to the escape of partial surface oxygen atoms to form oxygen defects. Generally, the coordination-unsaturated atoms at the steps, corners, kinks and edges of materials with more dangling bonds are prone to act as active sites.[18] The atoms with abundant dangling bonds along the crooked surface or near oxygen defects on the surface favors the increase of active sites. Simultaneously, the surface oxygen defects can also serve as surface separation centers for charge carriers, promoting the utilization efficiency of surface-arrived charge carriers.

As a proof-of-concept demonstration, the layered $Bi_{12}O_{17}Cl_2$ is selected as a model system to perform investigation. The oxygen defect modified $Bi_{12}O_{17}Cl_2$ superfine nanotube with bilayer thickness of tube wall is constructed. Taking advantage of ultrathin tube wall for fast bulk charge diffusion, tubular structure to accelerate surface charge separation and oxygen defects for effective CO_2 activation, the $Bi_{12}O_{17}Cl_2$ nanotubes delivers a striking 16.8 times improved photocatalytic activity than bulk $Bi_{12}O_{17}Cl_2$ towards converting CO_2 to CO.

Transmission electron microscopy (TEM) results of $Bi_{12}O_{17}Cl_2$ nanotubes reveal a clean, freestanding tube-like morphology with the average tube diameter around 6.2 nm (Figure S1a, b). From the enlarged image, the thickness of most tube wall was 2 layers (Figure S1c, d). Particularly, the surface microstructure and local atomic structure are further studied by aberration-corrected scanning transmission electron microscopy using the high-angle annular dark field imaging technique (STEM-HAADF). As depicted in Figure 1a and 1b, this system displays a freestanding superfine tube-like morphology. The tube diameter is about 6 nm and the near transparency in tube center shows its ultrathin thickness of tube wall (Figure 1b, 1c). The partly

distorted lattice can be observed due to the curved structure and existed oxygen defects (Figure 1d).[7] From the enlarged image, the thickness of tube wall is 2 layers (Figure 1c, 1e). The measured exterior bismuth interatomic distance is 0.408 nm, much larger than that of 0.389 nm in BiOCl (Figure 1e, 1f). The HAADF-STEM-EDS elemental mapping of $Bi_{12}O_{17}Cl_2$ nanotubes further suggests the uniformly distribution of Bi, O, Cl elements (Figure S2). These results give solid direct evidence for the artificial synthesis of clean and freestanding $Bi_{12}O_{17}Cl_2$ nanotubes with bilayer tube wall thickness.

The XRD pattern can be readily indexed to the tetragonal $Bi_{12}O_{17}Cl_2$ (JCPDS No. 37-0702), suggesting the $Bi_{12}O_{17}Cl_2$ materials have been prepared successfully (Figure 2a).[19] The weak peak intensity and larger half peak width meaning the poor crystallinity, in good agreement with the superfine nanotubes with ultrathin thickness. To determine the formation of oxygen defects, the low-temperature electron paramagnetic resonance (EPR) analysis is performed as it can afford valuable fingerprinting information regarding the trapped electrons and surface defects in materials. The $Bi_{12}O_{17}Cl_2$ samples displays an EPR signal at g = 2.001 (Figure 2b), which can be assigned to the electrons trapped on oxygen defects.[10] However, the $Bi_{12}O_{17}Cl_2$ nanotubes exhibits the greatly enhanced signal intensity than bulk $Bi_{12}O_{17}Cl_2$ (characterizations of bulk $Bi_{12}O_{17}Cl_2$ are shown in Figure S3-S5), revealing the $Bi_{12}O_{17}Cl_2$ nanotubes possess much higher oxygen defect concentration. XPS O 1s core level spectra is shown in Figure 2c with two peaks located at 529.7 and 531.0 eV. The band energy at 529.7 eV is deemed as the oxygen bond of Bi-O-Bi while the peak at 531.0 eV can be assigned to a high number of defect sites with a low oxygen coordination.[20] The area of the peak at 531.0 eV for $Bi_{12}O_{17}Cl_2$ nanotubes is larger than that of bulk counterparts, revealing the $Bi_{12}O_{17}Cl_2$ nanotubes have more oxygen defects, further testified by surface charge revealed by zeta-potentials. The zeta potentials change from -4.8 mV for bulk $Bi_{12}O_{17}Cl_2$ to +24.0 mV for the $Bi_{12}O_{17}Cl_2$ nanotubes, which suggests the increased oxygen defect concentrations can attract more positive charge on the surface.[21] In order to determine the structure differences of the samples, Raman spectroscopy has been carried out (Figure 2d). The A_{1g} and E_g modes

of Bi-Cl bond stretching mode at about 131 cm^{-1} in bulk $Bi_{12}O_{17}Cl_2$ shifts to 139 cm^{-1} for $Bi_{12}O_{17}Cl_2$ nanotubes. The peak at 95 cm^{-1} is ascribed to the A_{1g} internal Bi-Cl stretching mode, while its ratio in bulk $Bi_{12}O_{17}Cl_2$ is much higher than that in $Bi_{12}O_{17}Cl_2$ nanotubes. Together with the result of STEM-HAADF, TEM, XRD, EPR and XPS, it suggests the bilayer $Bi_{12}O_{17}Cl_2$ nanotubes with abundant oxygen defects have been obtained which provide an ideal structure to boost the CO_2 photoreduction activity. The tubular structure will inevitable result in surface structure distortion and atoms with more dangling bonds be formed. At the same time, the partial higher electron density in oxygen defects is favorable to adsorption and activation of CO_2. Therefore, the atoms with abundant dangling bonds along the crooked surface or near oxygen defects are preferable to be active sites for CO_2 reduction.

It has been widely accepted that energy band structure of semiconductors will greatly affect the photocatalytic behavior. The photoresponse range of the $Bi_{12}O_{17}Cl_2$ nanotubes and bulk counterpart is determined by UV-Vis absorption spectra (Figure 3a). Due to the quantum confinement effect, the onset absorption edge of $Bi_{12}O_{17}Cl_2$ nanotubes displays blue shift relative to bulk $Bi_{12}O_{17}Cl_2$.[11] However, the shoulder and tail absorption in $Bi_{12}O_{17}Cl_2$ nanotubes appears, which is derived from the abundant surface oxygen defects.[22] The band gap of the $Bi_{12}O_{17}Cl_2$ nanotubes is calculated to be about 2.36 eV, which is slightly larger than that of bulk $Bi_{12}O_{17}Cl_2$ (2.25 eV) (Figure 3b). The relative positions of valence band (VB) maximum for samples are determined by XPS valence spectra. As shown in Figure 3c, the $Bi_{12}O_{17}Cl_2$ nanotubes displays more positive location (1.56 eV) than that of bulk $Bi_{12}O_{17}Cl_2$ (1.40 eV). Thus, it is reasonable to infer that its conduction band (CB) minimum is -0.8 and -0.85 eV of $Bi_{12}O_{17}Cl_2$ nanotubes and bulk $Bi_{12}O_{17}Cl_2$, respectively, as schematically illustrated in Figure 3d. It is important to note that the downshifted CB position of $Bi_{12}O_{17}Cl_2$ nanotubes still meet the thermodynamic demands for CO_2 reduction. Generally, the electrons on the higher CB position have stronger reduction power, thus the CO_2 is easier to be activated to produce carbon-based fuels. In this system, the $Bi_{12}O_{17}Cl_2$ nanotubes possess more positive CB potential, thereby the increased CO_2 photoreduction activity may be not dominated by the CB potential.

To disclose the role of unique tubular structure with bilayer thickness and surface oxygen defects in affecting photocatalysis, the solar CO_2 reduction experiments are performed in water without cocatalyst and sacrifice reagent under the irradiation of 300 W Xe lamp. The dominant product is determined to be CO accompanied by a trace amount of methane. The CO yield gradually improved with the illumination time, and the total yield of CO achieved during 4 h reaction is 194.5 μmol g^{-1} (Figure 4a). The average CO-generation rate of $Bi_{12}O_{17}Cl_2$ nanotubes is up to 48.6 μmol g^{-1} h^{-1}, which is 16.8 times higher than that of the bulk $Bi_{12}O_{17}Cl_2$ (2.9 μmol g^{-1} h^{-1}), revealing the giant increased photocatalytic activity of the $Bi_{12}O_{17}Cl_2$ nanotubes. During the CO_2 photoreduction process, $Bi_{12}O_{17}Cl_2$ nanotubes can simultaneously realize H_2O oxidation into O_2 with an average O_2 evolution rates of about 23 μmol g^{-1} h^{-1}. The control experiments in dark, without photocatalysts or in Ar did not show the generation of CO, demonstrating the CO is formed by CO_2 reduction over $Bi_{12}O_{17}Cl_2$ under light irradiation. Moreover, the ^{13}C isotope labelling experiment is performed over $Bi_{12}O_{17}Cl_2$ nanotubes using $^{13}CO_2$ as substrate to explore the source of carbon. As shown in Figure 4c, the peak at m/z = 29 in the mass spectra can be assigned to ^{13}CO, suggesting that the carbon source of CO is derive from the used CO_2. This superior CO-generation rate over $Bi_{12}O_{17}Cl_2$ nanotubes is also outperform to many reported results, such as oxygen vacancies-rich BiOCl,[16] zinc vacancies-rich one-unit-cell $ZnIn_2S_4$,[21] partially oxidized SnS_2 atomic layers,[23] defect-rich ZnAl-LDH,[12] carbon-doped BN nanosheets,[24] α-Fe_2O_3/g-C_3N_4,[25] and UiO-66/C_3N_4 nanosheets.[26] More importantly, no significant loss of photocatalytic activity can be observed after three cycle testing, suggesting the stability (Figure 4b). XRD, TEM, XPS and EPR analysis in Figure S6 further demonstrate the structure of the $Bi_{12}O_{17}Cl_2$ nanotubes does not occur any obvious variation after photoreduction cycle test, certifying its favorable photostability. The apparent quantum efficiency of $Bi_{12}O_{17}Cl_2$ nanotubes at 400 nm is calculated to be 0.14% within 6 h.

To insight the origin of increased CO yield, the interfacial adsorption, charge separation and CO desorption process are detail studied since they are crucial factors essentially determining the efficiency of photocatalysis. It is widely accepted that a

larger specific surface area can adsorb more reactant. The $Bi_{12}O_{17}Cl_2$ nanotubes displays much higher BET specific surface area than bulk $Bi_{12}O_{17}Cl_2$ (16.36 vs 3.73 m^2/g) (Figure S7), which favors the photocatalytic process. The CO_2 adsorption is consider as the prerequisite for CO_2 photoreduction, therefore the CO_2 adsorption isotherms are further determined (Figure 4d). The $Bi_{12}O_{17}Cl_2$ nanotubes displays a 3.4 times higher CO_2 adsorption amount than that of bulk $Bi_{12}O_{17}Cl_2$, suggests the effective adsorption of CO_2. Moreover, the abundant surface oxygen defects in $Bi_{12}O_{17}Cl_2$ nanotubes are conducive to the CO_2 adsorption and activation to form $CO_2^{\bullet-}$ intermediate.[12, 16] Contact-angle measurement suggest hydrophilicity is not the dominated factor to affect CO_2 photoreduction process (Figure S8).

To study the migration and recombination process of photogenerated charge carriers, the time-resolved transient photoluminescence (PL) spectra are performed (Figure 4d).[26] The decay kinetic of $Bi_{12}O_{17}Cl_2$ nanotubes is much slower than that of bulk $Bi_{12}O_{17}Cl_2$, in which the average lifetimes are determined to be 11.38 and 3.55 ns, respectively. This greatly prolonged lifetime suggests the $Bi_{12}O_{17}Cl_2$ nanotubes have higher charge separation efficiency. Three features may account for the greatly improved charge separation efficiency, namely bilayer thickness of tube wall, tubular structure and abundant surface oxygen defects. The ultrathin thickness of tube wall guarantees the rapid migration of charge carriers from the material interior to the surface, while the charge carriers in bulk materials will be more likely to be lost due to recombination.[18] At the same time, the generated electrons will to migrate along the $[Cl_2]$ slices to $[Bi_{12}O_{17}]$ slices (perpendicular to nanotube direction) due the internal static electric fields, while the holes will transfer along the $[Cl_2]$ slices to the material edges.[19, 27] Since the nanotube structure and the $[Cl_2]$ slices is along with the tube direction (from STEM image), the generated holes will self-accelerating transfer along the nanotubes. The directional conduction function of $Bi_{12}O_{17}Cl_2$ nanotubes for holes enable the effective charge separation. In addition, the surface oxygen defects can serve as surface separation centers for charge carriers and further increases the lifetime of the carriers. Moreover, the greatly decreased PL intensity of $Bi_{12}O_{17}Cl_2$ nanotubes in steady-state PL spectra and smaller resistance in electrochemical impedance spectra

10.1002/anie.201809492

also suggest the better electrical conductivity and more efficient charge separation (Figure. S9).

According to the previous reports, the reaction mechanism of CO_2 reduction to yield CO in H_2O can be presented as follows:[23]

$$CO_2\ (g) \rightarrow CO_2^* \quad (1a)$$

$$H_2O \rightarrow H^+ + OH^- \quad (1b)$$

$$CO_2^* + H^+ + e^- \rightarrow COOH^* \quad (2)$$

$$COOH^* + H^+ + e^- \rightarrow CO^* + H_2O \quad (3)$$

$$CO^* \rightarrow CO \quad (4)$$

where "*" means the corresponding adsorption state on the surface. To deeply insight into CO_2 photoreduction process over $Bi_{12}O_{17}Cl_2$ nanotubes, in situ Fourier transform infrared spectroscopy (FTIR) is carried out (Figure 4f). The peaks at 1609 and 1340 cm^{-1} were assigned to the asymmetric and symmetric OCO stretches of b-CO_3^{2-} groups, respectively. A new IR peak around 1565 cm^{-1} appears and the intensity gradually increased with the extended irradiation time, in which it can be ascribed to COOH* intermediate, revealing the activation and reaction of adsorbed CO_2. Additionally, CO desorption process is also an important factor to determine whole CO_2 photoreduction performance. To assess the CO desorption performance, the CO temperature-programmed desorption (TPD) measurements are performed (Figure S10). The lower CO onset desorption temperature and higher total amount of detected CO for $Bi_{12}O_{17}Cl_2$ nanotubes suggests the formed CO* molecules can deviate from the surface of $Bi_{12}O_{17}Cl_2$ nanotubes much easier, which enables the efficient and sustaining production of CO.

In conclusion, bilayer $Bi_{12}O_{17}Cl_2$ nanotubes with abundant surface oxygen defects has been prepared. Compared to the bulk counterparts, the $Bi_{12}O_{17}Cl_2$ nanotubes displays improved CO_2 reduction property under solar light irradiation. The unique tubular structure with ultrathin thickness and defects-rich enable the $Bi_{12}O_{17}Cl_2$ nanotubes with improved adsorption and activation of CO_2, increased charge separation efficiency, and better CO liberation from catalyst, optimizing the CO_2 photoreduction activity to yield CO. In brief, this study may open new opportunities for designing other catalysts with similar structure for highly efficient solar driven CO_2 reduction.

Acknowledgements

This work is supported by the National Natural Science Foundation of China (No. 21676128, 21576123, 21476098, 11504046). This work also supported by MOE Tier 1 grant RG4/17, MOE Tier 2 grant MOE2016-T2-1-131, Singapore National Research Foundation under NRF award number NRF-RF2013-08.

References

[1] P. Zhang, T. Wang, J. L. Gong, *Adv. Mater.* **2015**, *27*, 5328-5342.

[2] C. Steinlechner, H. Junge, *Angew. Chem. Int. Ed.* **2018**, *57*, 44-45.

[3] P. Li, Y. Zhou, Z. Y. Zhao, Q. F. Xu, X. Y. Wang, M. Xiao, Z. G. Zou, J. *Am. Chem. Soc.* **2015**, *137*, 9547.

[4] S. Gao, Y. Lin, X. C. Jiao, Y. F. Sun, Q. Q. Luo, W. H. Zhang, D. Q. Li, J. L. Yang, Y. Xie, *Nature* **2016**, *529*, 68-71.

[5] D. H. Deng, K. S. Novoselov, Q. Fu, N. F. Zheng, Z. Q. Tian, X. H. Bao, *Nat. Nanotechnol.* **2016**, *11*, 218-230.

[6] F. Song, X. L. Hu, *Nat. Commun.* **2014**, *5*, 4477.

[7] Y. F. Zhao, Y. X. Zhao, G. I. N. Waterhouse, L. R. Zheng, X. Z. Cao, F. Teng, L. Z. Wu, C. H. Tung, D. O'Hare, T. R. Zhang, *Adv. Mater.* **2017**, *29*, 1703828.

[8] J. Di, J. X. Xia, M. X. Ji, L. Xu, S. Yin, Z. G. Chen, H. M. Li, *J. Mater. Chem. A* **2016**, *4*, 5051-5061.

[9] Q. H. Liang, Z. Li, Z. H. Huang, F. Y. Kang, Q. H. Yang, *Adv. Funct. Mater.* **2015**, *25*, 6885-6892.

[10] F. C. Lei, Y. F. Sun, K. T. Liu, S. Gao, L. Liang, B. C. Pan, Y. Xie, *J. Am. Chem. Soc.* **2014**, *136*, 6826-6829.

[11] L. Liang, F. C. Lei, S. Gao, Y. F. Sun, X. C. Jiao, J. Wu, S. Qamar, Y. Xie, *Angew. Chem. Int. Ed.* **2015**, *54*, 13971-13974.

[12] Y. F. Zhao, G. B. Chen, T. Bian, C. Zhou, G. I. N. Waterhouse, L. Z. Wu, C. H. Tung, L. J. Smith, D. O'Hare, T. R. Zhang, *Adv. Mater.* **2015**, *27*, 7824-7831.

[13] W. L. Yang, L. Zhang, J. F. Xie, X. D. Zhang, Q. H. Liu, T. Yao, S. Q. Wei, Q. Zhang, Y. Xie, *Angew. Chem. Int. Ed.* **2016**, *55*, 6716-6720.

[14] H. Li, J. Shang, Z. H. Ai, L. Z. Zhang, *J. Am. Chem. Soc.* **2015**, *137*, 6393-6399.

[15] N. Zhang, X. Y. Li, H. C. Ye, S. M. Chen, H. X. Ju, D. B. Liu, Y. Lin, W. Ye, C.M. Wang, Q. Xu, J. F. Zhu, L. Song, J. Jiang, Y. J. Xiong, *J. Am. Chem. Soc.* **2016**, *138*, 8928-8935.

[16] L. Zhang, W. Z. Wang, D. Jiang, E. P. Gao, S. M. Sun, *Nano Res.* **2015**, *8*, 821-831.

[17] J. Di, J. Xiong, H. M. Li, Z. Liu, *Adv. Mater.* **2018**, *30*, 1704548.

[18] Y. F. Sun, S. Gao, F. C. Lei, Y. Xie, *Chem. Soc. Rev.* **2015**, *44*, 623-636.

[19] J. Li, G. M. Zhan, Y. Yu, L. Z. Zhang, *Nat. Commun.* **2016**, *7*, 11480.

[20] J. Bao, X. D. Zhang, B. Fan, J. J. Zhang, M. Zhou, W. L. Yang, X. Hu, H. Wang, B. C. Pan, Y. Xie, *Angew. Chem. Int. Ed.* **2015**, *54*, 7399-7404.

[21] X. C. Jiao, Z. W. Chen, X. D. Li, Y. F. Sun, S. Gao, W. S. Yan, C. M. Wang, Q. Zhang, Y. Lin, Y. Luo, Y. Xie, *J. Am. Chem. Soc.* **2017**, *139*, 7586-7594.

[22] H. Li, J. G. Shi, K. Zhao, L. Z. Zhang, *Nanoscale* **2014**, *6*, 14168-14173.

[23] X. C. Jiao, X. D. Li, X. Y. Jin, Y. F. Sun, J. Q. Xu, L. Liang, H. X. Ju, J. F. Zhu, Y. Pan, W. S. Yan, Y. Lin, Y. Xie, *J. Am. Chem. Soc.* **2017**, *139*, 18044-18051.

[24] C. J. Huang, C. Chen, M. W. Zhang, L. H. Lin, X. X. Ye, S. Lin, M. Antonietti, X. C. Wang, *Nat. Commun.* **2015**, *6*, 7698.

[25] Z. F. Jiang, W. M. Wan, H. M. Li, S. Q. Yuan, H. J. Zhao, P. K. Wong, *Adv. Mater.* **2018**, *30*, 1706108.

[26] L. Shi, T. Wang, H. B. Zhang, K. Chang, J. H. Ye, *Adv. Funct. Mater.* **2015**, *25*, 5360-5367.

[27] S. Bai, X. Y. Li, Q. Kong, R. Long, C. M. Wang, J. Jiang, Y. J. Xiong, *Adv. Mater.* **2015**, *27*, 3444-3452.

10.1002/anie.201809492

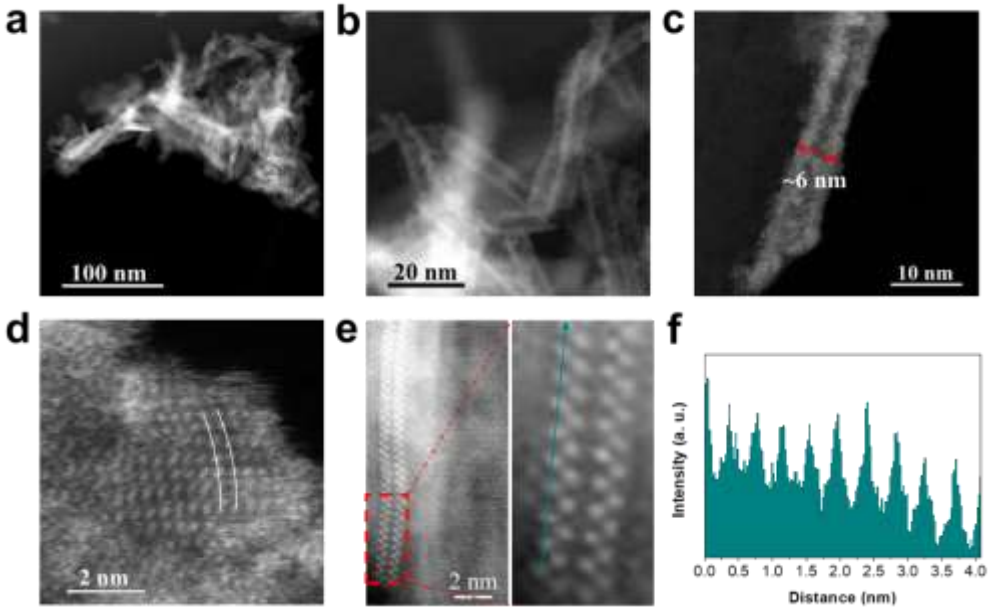

Figure 1. (a-e) Aberration-corrected HAADF-STEM images of $Bi_{12}O_{17}Cl_2$ nanotubes, (f) intensity profile corresponding to the dark cyan arrow in e.

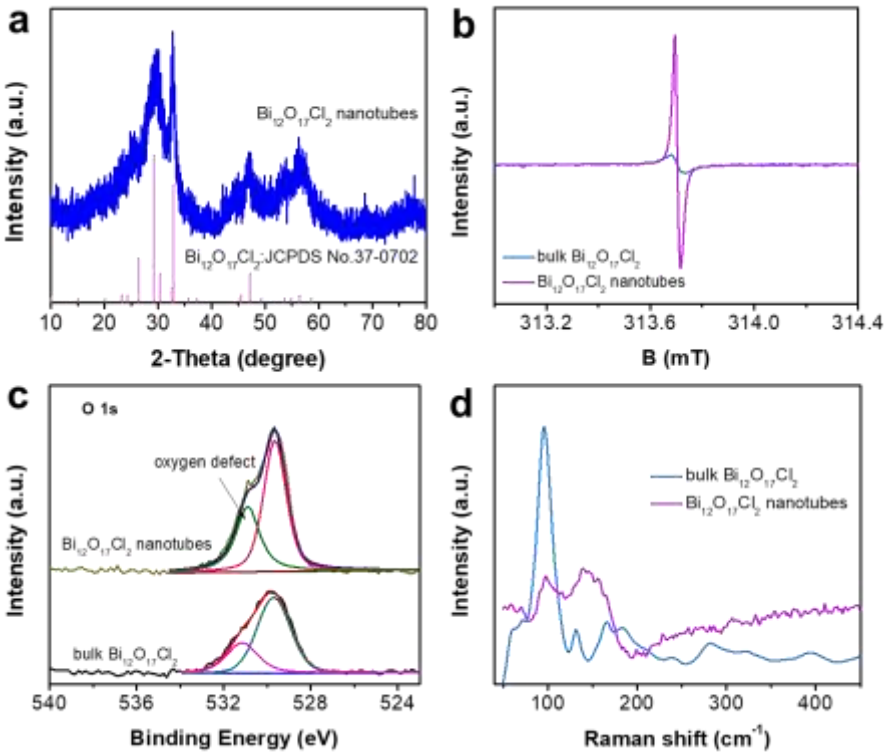

Figure 2. Characterizations for $Bi_{12}O_{17}Cl_2$ nanotubes and bulk $Bi_{12}O_{17}Cl_2$: (a) XRD patterns, (b) EPR, (c) O 1s XPS spectra, (d) Raman spectra.

10.1002/anie.201809492

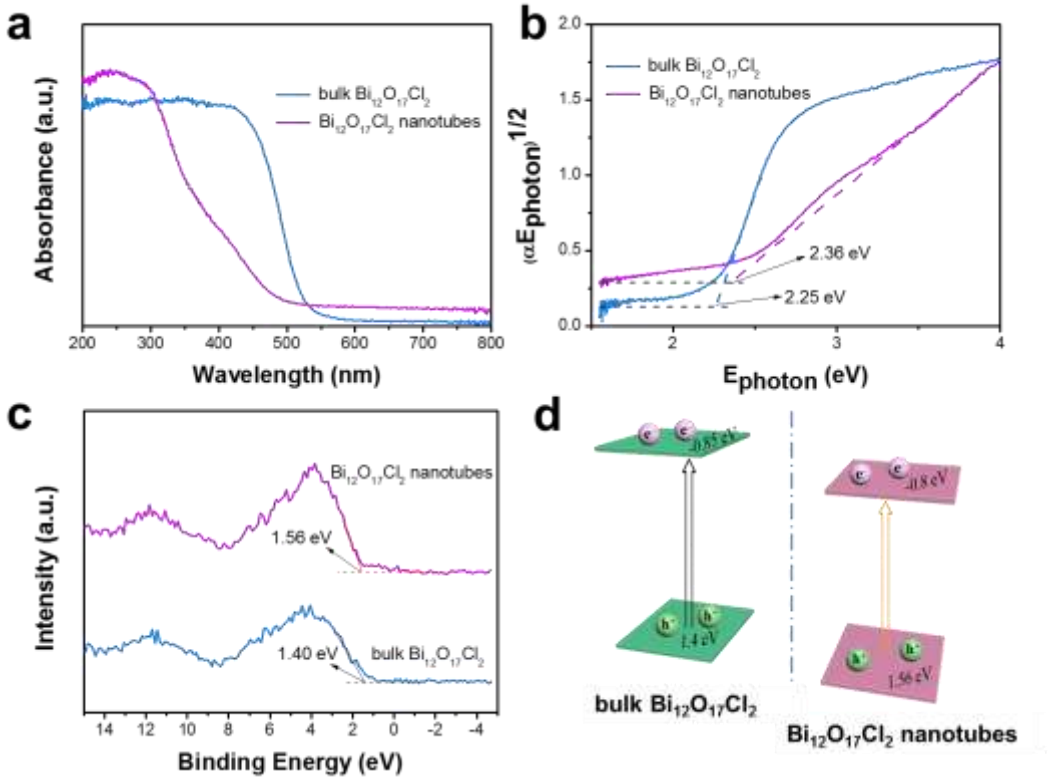

Figure 3. (a) UV-vis spectra, (b) $(\alpha E_{photon})^{1/2}$ vs E_{photon} curves, (c) XPS valence spectra of the $Bi_{12}O_{17}Cl_2$ samples, (d) schematic band structure obtained according to the results in (b) and (c).

10.1002/anie.201809492

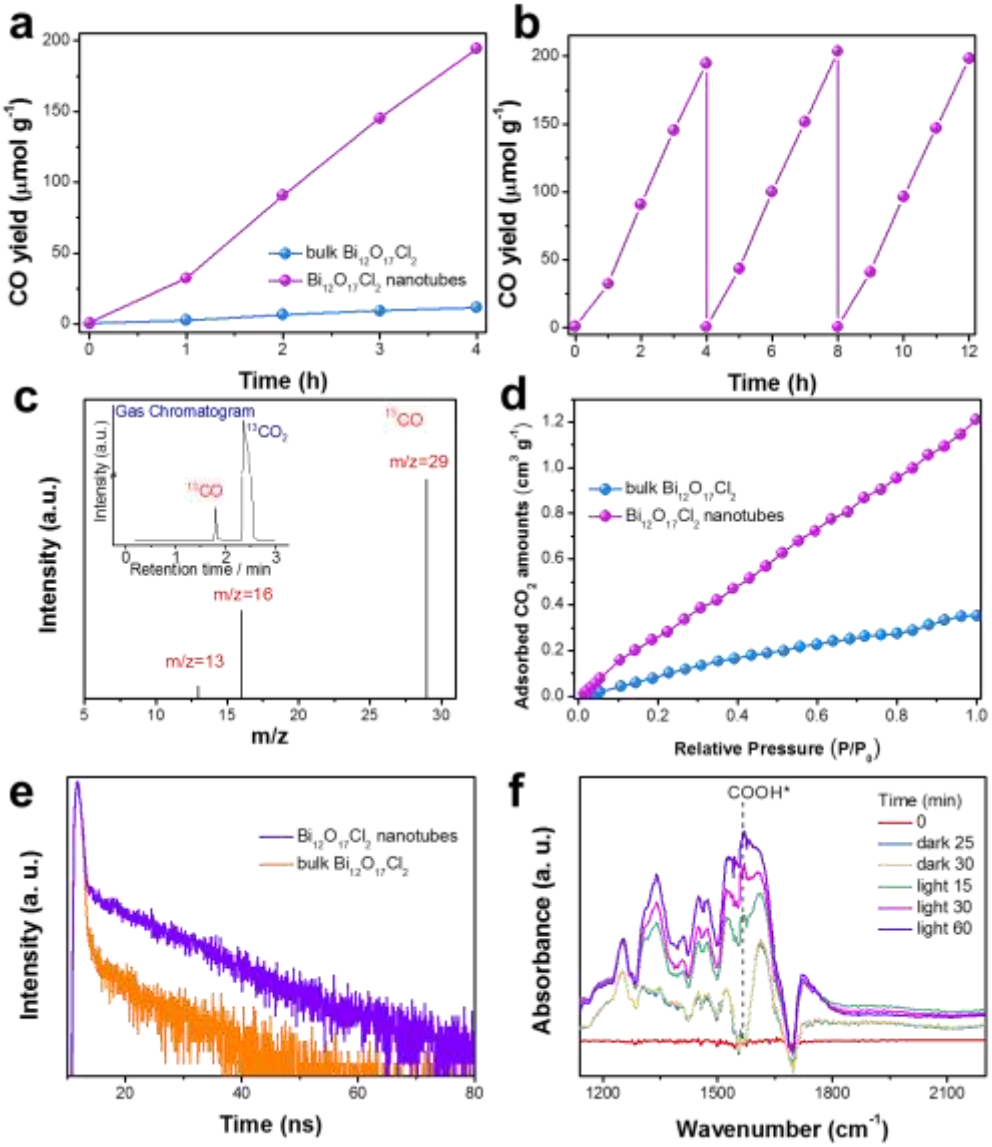

Figure 4. (a) Photoreduction of CO_2 into CO over $Bi_{12}O_{17}Cl_2$ samples, (b) photocatalytic stability of $Bi_{12}O_{17}Cl_2$ nanotubes, (c) mass spectra of ^{13}CO (m/z = 29) produced over $Bi_{12}O_{17}Cl_2$ nanotubes, (d) CO_2 adsorption isotherms, (e) time-resolved transient PL decay, (f) in situ FTIR spectra for the adsorption and activation of CO_2 on $Bi_{12}O_{17}Cl_2$ nanotubes.

10.1002/anie.201809492

TOC

Defect-rich $Bi_{12}O_{17}Cl_2$ superfine nanotubes were prepared for the photocatalytic reduction of CO_2. Benefiting from the superfine nanotube structure to accelerate charge separation and oxygen defects to facilitate CO_2 activation, the $Bi_{12}O_{17}Cl_2$ nanotubes displayed a CO formation rate of 48.6 μmol g^{-1} h^{-1} in water without cocatalyst and sacrifice reagent, roughly 16.8 times than that of bulk $Bi_{12}O_{17}Cl_2$.